molecular pharmaceutics

Article

pubs.acs.org/molecularpharmaceutics

Biodistribution and *in Vivo* Activities of Tumor-Associated Macrophage-Targeting Nanoparticles Incorporated with Doxorubicin

Mengmeng Niu,[†] Youssef W. Naguib,[†] Abdulaziz M. Aldayel,[†] Yan-chun Shi,[‡] Stephen D. Hursting,[§] Matthew A. Hersh,[∥] and Zhengrong Cui*[,†,‡]

[†]College of Pharmacy, Pharmaceutics Division, The University of Texas at Austin, Austin, Texas 78712, United States

[‡]Inner Mongolia Key Laboratory of Molecular Biology, Inner Mongolia Medical University, Hohhot, Inner Mongolia, China

[§]Gillings School of Global Public Health, University of North Carolina, Chapel Hill, North Carolina 27599, United States

[∥]College of Natural Sciences, Division of Statistics and Scientific Computation, The University of Texas at Austin, Austin, Texas 78712, United States

Supporting Information

ABSTRACT: Tumor-associated macrophages (TAMs) are increasingly considered a viable target for tumor imaging and therapy. Previously, we reported that innovative surface-functionalization of nanoparticles may help target them to TAMs. In this report, using poly(lactic-*co*-glycolic) acid (PLGA) nanoparticles incorporated with doxorubicin (DOX) (DOX-NPs), we studied the effect of surface-modification of the nanoparticles with mannose and/or acid-sensitive sheddable polyethylene glycol (PEG) on the biodistribution of DOX and the uptake of DOX by TAMs in tumor-bearing mice. We demonstrated that surface-modification of the DOX-NPs with both mannose and acid-sensitive sheddable PEG significantly increased the accumulation of DOX in tumors, enhanced the uptake of the DOX by TAMs, but decreased the distribution of DOX in mononuclear phagocyte system (MPS), such as liver. We also confirmed that the acid-sensitive sheddable PEGylated, mannose-modified DOX-nanoparticles (DOX-AS-M-NPs) targeted TAMs because depletion of TAMs in tumor-bearing mice significantly decreased the accumulation of DOX in tumor tissues. Furthermore, in a B16-F10 tumor-bearing mouse model, we showed that the DOX-AS-M-NPs were significantly more effective than free DOX in controlling tumor growth but had only minimum effect on the macrophage population in mouse liver and spleen. The AS-M-NPs are promising in targeting cytotoxic or macrophage-modulating agents into tumors to improve tumor therapy.

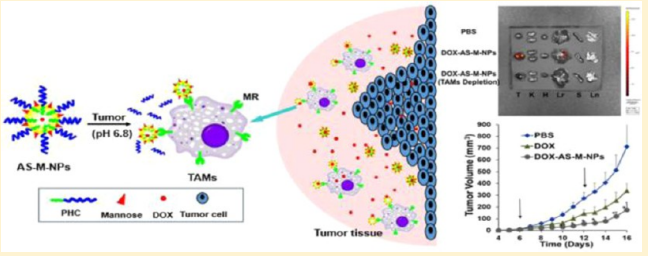

KEYWORDS: *cell uptake, ex vivo imaging, macrophage depletion, tumor growth inhibition, immunohistochemical staining*

INTRODUCTION

Numerous studies have revealed the importance of TAMs on tumor growth and development.[1−4] TAMs are innate immune effector cells recruited to tumor tissues.[5] They are present in both tumor stroma and nests,[6,7] accounting for up to 50% of tumor mass.[8] TAMs contribute to tumor growth by producing stromal breakdown factors and by suppressing adaptive immunity.[9] Moreover, TAMs induce chemoresistance by inhibiting tumor cell apoptosis.[10] Recently, there is also compelling evidence that TAM infiltration in tumors is correlated with poor prognosis of many cancers, including breast, pancreatic, ovarian, prostate, cervix, bladder cancer, and certain types of glioma and lymphoma in patients.[11−17] TAMs are thus considered a potentially viable target in designing innovative imaging and therapy strategies. In fact, there are various reported methods to target TAMs. Among them, using the membrane receptors on TAMs is commonly explored.[18−21] For example, the endocytic CD163 protein was recently proposed as a TAM target for anticancer and antiangiogenesis drug design.[22] Folate receptor-β, another protein commonly expressed on the surface of macrophages, had also been exploited to target toxins to TAMs.[23,24] Because TAMs overexpress mannose receptor (MR),[25] there had been efforts to increase the delivery of oligos, DNA, imaging agents, and vaccines to TAMs by surface-modifying the delivery systems with mannose derivatives,[26,27] anti-MR nanobody,[28] or galactose derivative.[29] Unfortunately, many of the previously reported delivery systems can be inevitably taken up by macrophages that are not in tumors because those macrophages often express similar membrane receptors as the TAMs do.[30]

To address this issue, we recently constructed an acid-sensitive sheddable PEGylated, mannose-modified nanoparticle platform (AS-M-NPs). The nanoparticles are prepared with PLGA, surface-modified with mannose, and PEGylated with an acid-sensitive PEG amphiphile, PEG-hydrazone-C18 (or PHC),

Received: August 18, 2014
Revised: October 7, 2014
Accepted: October 14, 2014
Published: October 14, 2014

which was synthesized by conjugating PEG (molecular weight, 2000) with stearic hydrazide using a hydrazone bond.[31] It was theorized that upon intravenous (i.v.) injection, the long flexible PEG chains shield the mannose on the surface of the nanoparticles and prevent the interaction of the nanoparticles with macrophages before the nanoparticles reach tumors. Once the nanoparticles accumulate in tumors by the enhanced permeability and retention (EPR) effect,[32] however, the slightly acidic tumor microenvironment (~ pH 6.84)[33] helps catalyze the hydrolysis of the hydrazone bond and facilitate the shedding of the PEG chains, exposing the mannose for interaction with MRs on the surface of TAMs. Previously, we showed fluorescence images of the histological sections of tumors in mice injected with fluorescein-labeled AS-M-NPs, which indicated that the AS-M-NPs can potentially target TAMs.[34] However, direct evidence is needed to demonstrate that the AS-M-NPs can indeed target TAMs.

In the present report, we present *ex vivo* fluorescence imaging data to demonstrate that surface-modification of PLGA nanoparticles incorporated with the self-fluorescent DOX with acid-sensitive sheddable PEG and mannose can effectively target the DOX into tumors by interacting with TAMs. Moreover, by taking advantage of the cytotoxicity of DOX, we showed that the DOX-AS-M-NPs were more effective than free DOX in inhibiting tumor growth. The DOX-AS-M-NPs significantly decreased TAM population in tumors, but showed only minimum effect on macrophages in mouse MPS organs such as liver and spleen.

MATERIALS AND METHODS

Materials. O-Stearoyl mannose (M-C18), polyethylene glycol 2000-hydrazone-C18 (PHC), and polyethylene glycol 2000-amide-C18 (PAC) were synthesized following our previously published methods.[31,34] Doxorubicin hydrochloride was from Fisher Scientific Co. (Pittsburgh, PA). Zoledronic acid, 3-(4,5-dimethylthiazol-2-yl)-2,5-diphenyltetrazolium bromide (MTT), PLGA (752H), and poly-D-lysine were from Sigma-Aldrich (St. Louis, MO). Mannose was from Tokyo Chemical Industry Co., Ltd. (Portland, OR). Hematoxylin-eosin (H&E) and anti-CD31 antibody were from Abcam (Cambridge, MA). Hoechst 33342 was from AnaSpec, Inc. (Fremont, CA). The 5-bromo-2′-deoxyuridine (BrdU) and primary BrdU monoclonal antibody were from BD Biosciences (San Jose, CA). Anti-CD206, RM0029-11H3, and FITC-labeled anti-CD206 antibody were from Santa Cruz Biotechnology, Inc. (Dallas, TX). Solvents used in chemical synthesis were of analytical grade.

Cells and Animals. J774A.1 macrophage cells, B16-F10 murine melanoma cells, BxPC-3 human pancreatic cancer cells, and TC-1 murine lung cancer cells were from American type Culture Collection (ATCC, Manassas, VA) and cultured in DMEM (or RPMI1640 for BxPC-3) at 37 °C and 5% CO_2. Media were supplemented with 10% fetal bovine serum (FBS), 100 U/mL of penicillin, and 100 μg/mL of streptomycin, all from Invitrogen (Carlsbad, CA). Female C57BL/6 mice (6−8 weeks) and male athymic nude mice were from Charles River Laboratories (Wilmington, MA). Animal studies were performed in accordance with the National Research Council guide for the care and use of laboratory animals. Animal protocol was approved by the Institutional Animal Care and Use Committee at The University of Texas at Austin.

Preparation and Characterization of Doxorubicin (DOX)-Loaded Nanoparticles. Nanoparticles were prepared following our previously reported method with slight modifications.[34] Briefly, 0.9 mL of tetrahydrofuran (THF) containing PLGA 752H (3 mg) and DOX (0.3 mg) was added dropwise into 4.5 mL of water under stirring. The nanoparticles were collected by centrifugation (13 000 × *g*, 10 min, 4 °C) after the evaporation of THF. For the purpose of surface modification, M-C18 (1.2 mg), PAC (1.2 mg), or PHC (3.6 mg) were dissolved together with PLGA and DOX in THF and added into water.[34] Particle sizes and zeta potentials of the nanoparticles were determined using a Malvern Zeta Sizer Nano ZS (Westborough, MA). The morphology of the nanoparticles was analyzed using a Zeiss Supra 40 VP Scanning Electron Microscope (SEM) (Zeiss SMT AG, Oberkochen, Germany) in the ICMB Microscopy and Imaging Facility at the University of Texas at Austin.[35] The entrapment efficiency (EE) of DOX was determined spectrophotometrically at 490 nm by measuring the amount of free unentrapped DOX in the external aqueous solution after centrifugation of the nanoparticles in suspension for 5 min at 13 000 × *g*. To determine the total amount of DOX in the nanoparticles, 500 μL of nanoparticles in suspension were mixed with 4.5 mL of dimethyl sulfoxide (DMSO) for 5 min by sonication, and the concentration of DOX was determined. The EE was calculated according to the following equation:

$$\mathrm{EE}(\%) = \left(\frac{\mathrm{DOX}_{\mathrm{total}} - \mathrm{DOX}_{\text{un-entrapped}}}{\mathrm{DOX}_{\mathrm{total}}}\right) \times 100\%$$

***In Vitro* Release of DOX from Nanoparticles.** The rate at which DOX was released from nanoparticles was measured as a function of time when the nanoparticles were incubated in phosphate-buffered saline (PBS, pH 7.4 or 6.8, 10 mM). Triplicate samples of 5 mg of nanoparticles were suspended in 0.5 mL of PBS and sonicated briefly in an ultrasonic water bath. The samples were then incubated in an orbital shaker at 37 °C, 100 rpm. At various time points, the particles were centrifuged at 13 000 × *g* for 5 min, and 100 μL of supernatant was removed and replaced with fresh PBS. The fluorescence intensity of DOX in the supernatant was measured using a BioTek Synery HT Multi-Mode Microplate Reader (Winooski, VT, USA) at excitation 470 nm/emission 590 nm to determine the DOX released from nanoparticles.

Intracellular Uptake of DOX by J774A.1 Cells. J774A.1 cells were seeded with a density of 5×10^5 cells per well on poly-D-lysine-precoated glass coverslips, placed inside wells of a 6-well tissue culture plate, and incubated overnight. On the second day, cell culture medium was replaced with 2.5 mL of 50 μM DOX in various nanoparticles (i.e., DOX-NPs, DOX-M-NPs, DOX-AI-M-NPs, and DOX-AS-M-NPs). Cells were incubated for 20 min, followed by five additional minutes of incubation with 50 μM Hoechst 33342 in a 37 °C incubator and protected from light. Cells were then washed with PBS three times, fixed with 4% paraformaldehyde, and observed under a fluorescence microscope (Olympus BX 53, Center Valley, PA) connected to the Olympus cellSens Dimension software. To investigate the effect of pH on the cellular uptake, nanoparticles were preincubated with PBS (pH 6.8) at 37 °C for 6 h before further incubating with cells.

In order to track the intracellular fate of nanoparticles, DOX-AS-M-NPs were prepared with 5% (w/w) of PLGA 752H that was conjugated with fluorescein isothiocyanate (FITC).[34] Cells were incubated with nanoparticles for 15, 30, or 60 min, followed by five additional minutes of incubation with Hoechst

A. Physical characteristics of various DOX-incorporated nanoparticles.

Nanoparticles	Surface modification	Particle size (nm)	Polydispersity index	Zeta potential (mV)	Entrapment efficient (%)
DOX-NPs	Without surface modification	132.4 ± 3.9	0.116 ± 0.006	-34.2 ± 2.2	73 ± 0.1
DOX-M-NPs	Mannose	136.7 ± 13.0	0.181 ± 0.004	-35.1 ± 2.3	66 ± 0.1
DOX-AI-M-NPs	Mannose, acid-insensitive PEG	145.7 ± 13.1	0.175 ± 0.010	-26.6 ± 1.8	64 ± 0.2
DOX-AS-NPs	Acid-sensitive PEG	138.4 ± 14.6	0.194 ± 0.076	-24.1 ± 4.5	70 ± 2.3
DOX-AS-M-NPs	Mannose, acid-sensitive PEG	151.2 ± 17.2	0.153 ± 0.008	-26.7 ± 1.6	63 ± 0.3

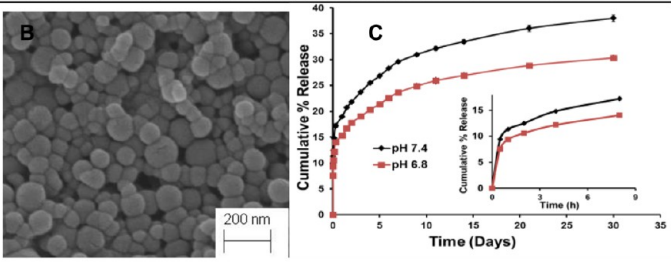

D. IC_{50} values (μg DOX/ml)

	B16-F10	J774A.1
DOX	0.09 ± 0.05 [a]	4.79 ± 0.61 [a]
DOX-NPs	3.12 ± 1.05 [b]	4.77 ± 1.55 [a]
DOX-M-NPs	2.69 ± 1.02 [b]	2.39 ± 0.41 [b]
DOX-AI-M-NPs	2.08 ± 0.30 [b]	3.76 ± 1.27 [a]
DOX-AS-M-NPs	2.23 ± 0.26 [b]	3.73 ± 0.59 [a]
*AS-M-NPs	178.70 ± 2.44 [c]	81.99 ± 2.20 [c]
DOX-AS-M-NPs, pH 6.8 incubation		1.75 ± 0.49 [d]

Figure 1. Characteristics of DOX-incorporated nanoparticles and their IC_{50} values. (A) Physical characteristics of various DOX-nanoparticles. (B) A representative SEM graph of DOX-AS-M-NPs. (C) The *in vitro* release profile of DOX from DOX-AS-M-NPs (inset, the release profile in the initial 8 h). (D) IC_{50} values of free DOX and various DOX-nanoparticles in B16-F10 cells and J774A.1 cells. As a control, the cytotoxicity of the DOX-free AS-M-NPs was also evaluated (*The IC_{50} values of the DOX-free AS-M-NPs are the equivalent DOX concentrations, if the AS-M-NPs were incorporated with DOX). Data in panels A, C, and D are mean ± SD ($n \geq 3$). In panel D, $^{a-d}p < 0.05$.

33342. Cells were then washed, fixed, and observed under a microscope as mentioned above.

***In Vitro* Cytotoxicity Assay.** B16-F10 cells (80% confluence) were plated at a cell density of 5×10^3 cells/well into 96-well plates. After 24 h of incubation at 37 °C with 5% CO_2, the growth medium was removed, and the cells were incubated for another 24 h with various DOX formulations, with DOX concentrations ranging from 0.001 to 10 μg/mL. Controls included cells incubated with DOX-free medium or blank nanoparticles (i.e., DOX-free AS-M-NPs). Cells were washed twice with PBS and incubated with 20 μL of MTT (5 mg/mL) solution for 4 h. Formazan crystals were solubilized with 150 μL of DMSO. The absorbance of each well at 570/630 nm was measured. Cell viability was calculated by comparing the absorbance with the untreated cells.

To evaluate the cytotoxicity of the DOX-NPs in macrophages, J774A.1 cells were seeded into 96-well plates at a cell density of 1×10^5 cells/well.[36] After 24 h of incubation, cells were treated with free DOX or various DOX-NPs, and cell viability was determined 24 h later using an MTT assay as mentioned above. Similarly, controls included cells incubated with DOX-free medium or DOX-free AS-M-NPs.

Biodistribution Studies. C57BL/6 mice were subcutaneously (s.c.) injected with B16-F10 cells (5×10^5/mouse) in the right flank. When tumors reached around 7 mm in diameter, mice were i.v. injected with PBS, free DOX solution, DOX-NPs, DOX-M-NPs, DOX-AI-M-NPs, DOX-AS-NPs, or DOX-AS-M-NPs (DOX dose, 10 mg/kg). Mice were euthanized 6 h later to collect blood, tumor, and major organs (e.g., heart, kidneys, liver, spleen, and lung). All samples were then imaged using an IVIS Spectrum (Caliper, Hopkinton, MA) (Em/Ex of 465/600 nm).

In order to evaluate the effect of TAMs on the uptake of the DOX-AS-M-NPs by tumors in mice, B16-F10 tumor-bearing C57BL/6 mice were intraperitoneally (i.p.) injected with zoledronic acid (5 mg/kg) 7 days after tumor cell injection to reduce macrophages in mice.[37] Zoledronic acid injection was repeated every 4 days for 4 more times. Two days after the last injection (i.e., 25 days after tumor cells injection), mice were i.v. injected with DOX-AS-M-NPs (DOX, 10 mg/kg). As controls, B16-F10 tumor-bearing mice that were not treated with zoledronic acid were i.v. injected with DOX-AS-M-NPs or sterile PBS. Mice were euthanized 6 h later to collect tumor and major organs for *ex vivo* imaging using IVIS Spectrum. Tumor tissues were also stained with RM0029-11H3, a macrophage marker, to confirm the reduction of TAMs by treatment with zoledronic acid.

Finally, to evaluate the kinetics of the biodistribution of the DOX-AS-M-NPs in mice, B16-F10 tumor-bearing mice were i.v. injected with DOX-AS-M-NPs (10 mg DOX/kg), and three mice were euthanized 6, 12, 24, or 48 h later to collect tumor, blood, and major organs, which were then imaged using the IVIS Spectrum.

For mice bearing BxPC-3 and TC-1 tumor, 2×10^6 or 5×10^5 cells were s.c. inoculated in athymic male nude mice or C57BL/6 mice, respectively. When tumor grew to around 7 mm in diameter, mice were grouped and i.v. injected with DOX-AS-M-NPs, free DOX, or sterile PBS. Mice were euthanized 6 h (BxPC-3 tumor-bearing mice) or 12 h (TC-1 tumor-bearing mice) later to collect tumors and major organs for *ex vivo* imaging.

***In Vivo* Antitumor Activity.** C57BL/6 mice were s.c. injected with B16-F10 cells (5×10^5/mouse) in the right flank on day 0. On day 6, mice were randomized ($n = 8$) and i.v. injected with PBS, free DOX solution, or DOX-AS-M-NPs. The dose of DOX was 5 mg/kg. Treatment was repeated on day 12. Tumor size and mouse body weight were monitored every day. Tumor volume was calculated using the following equation:[38] tumor volume = (length × width^2)/2. On day 16, mice were euthanized to collect tumor, liver, and spleen. Mice were i.p. injected with BrdU, 100 μg/g body weight, 30 min prior to euthanasia. Tissue samples were weighed and fixed for immunohistochemical staining. Tumor tissues were stained with H&E or anti-CD206, anti-CD31, or anti-BrdU antibodies. Liver and spleen tissues were sectioned and stained with RM0029-11H3.

Uptake of AS-M-NPs by Macrophages in B16-F10 Tumors. C57BL/6 mice were s.c. injected with 5×10^5 B16-

dx.doi.org/10.1021/mp500565q | *Mol. Pharmaceutics* 2014, 11, 4425−4436

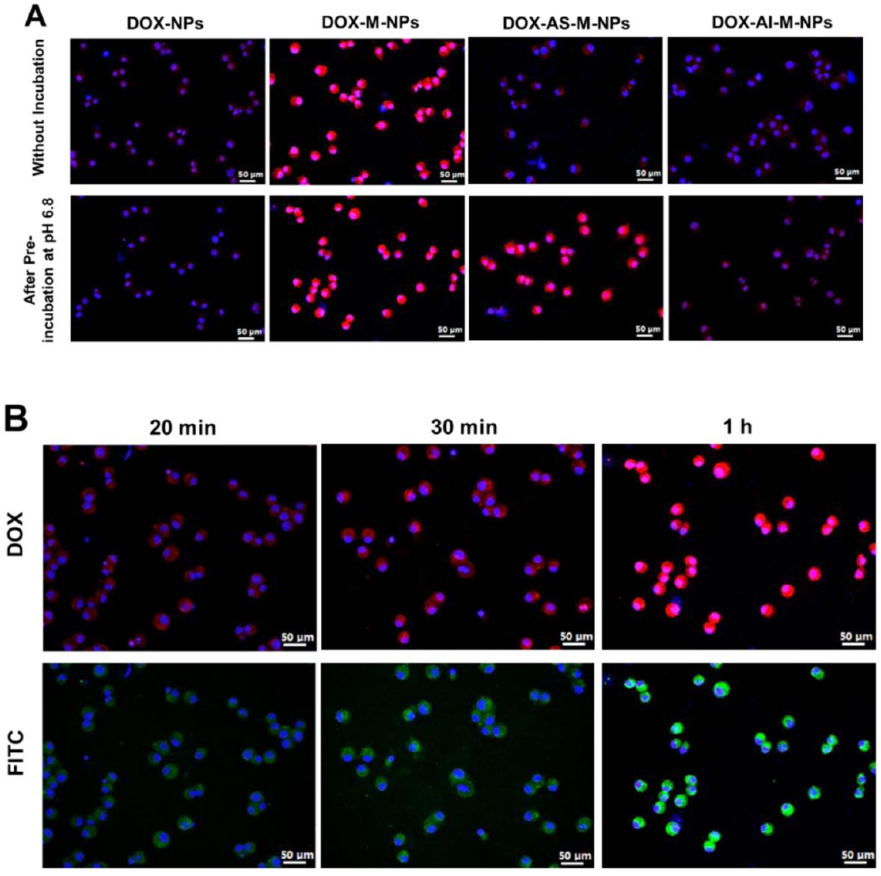

Figure 2. Uptake of DOX-incorporated nanoparticles by J774A.1 murine macrophages in culture. (A) Uptake of different DOX-nanoparticles (red) that were preincubated or not, at pH 6.8 for 6 h. Cells were incubated with DOX-nanoparticles for 20 min. (B) Intracellular location of DOX (red) or DOX-AS-M-NPs (green) after incubated with J774A.1 cells for 20 min, 30 min, or 1 h. Cell nuclei were stained with Hoechst (blue).

F10 cells. When tumors reached about 9 mm, mice were randomized and i.v. injected with PBS, free DOX, or various DOX-nanoparticles. The dose of DOX was 10 mg/kg. Mice were euthanized 6 h later to collect tumors. Tumor cell suspensions were stained with FITC-labeled anti-CD206 antibodies (1:200 dilution) for 20 min on ice and washed 3 times with PBS. Cells were then analyzed using a BD FACS Aria Flow Cytometer (San Jose, CA). The percent of $CD206^+$ cells that took up DOX (i.e., $DOX^+/CD206^+$%) was analyzed with the Flow Jo software (Tree Star Inc., Ashland, OR). Dead cells and cells debris were excluded based on the FSC-SSC plot. Live cells were then plotted in the green (FITC) vs red (DOX) dot plot quadrants. Double negative control was the tumor tissue single cell suspension from mice that were injected with sterile PBS. Positive control was the FITC-anti-CD206 stained tumor tissue single cells isolated from mice that were injected with sterile PBS. Positive control for the DOX was the tumor tissue single cell suspension from mice that were injected with sterile PBS, and the cells were coincubated with a DOX solution in culture for 20 min.

Statistics. Statistical analyses were completed by performing ANOVA followed by Fisher's protected least significant difference procedure. A P value of ≤ 0.05 (two-tail) was considered significant.

RESULTS

Preparation and Characterization of Doxorubicin-Loaded Nanoparticles with Various Surface Modifications. The following DOX-incorporated nanoparticles were prepared: DOX-NPs (DOX-incorporated PLGA nanoparticles without surface modification), DOX-M-NPs (DOX-NPs that were surface-modified with mannose but not PEGylated), DOX-AS-NPs (DOX-NPs that were PEGylated with acid-sensitive sheddable PEG, but not surface-modified with mannose), DOX-AS-M-NPs (DOX-NPs that were surface-modified with mannose and PEGylated with acid-sensitive sheddable PEG), and DOX-AI-M-NPs (DOX-NPs that were surface-modified with mannose and PEGylated with the acid-insensitive PEG2000-amide-C18) (Figure 1A). All DOX-loaded nanoparticles were around 130−150 nm in diameter, with a narrow size distribution (see polydispersity indices) (Figure 1A). The zeta potentials of DOX-loaded nanoparticles were −24 to −35 mV (Figure 1A). The entrapment efficiency of DOX was 60−70% (Figure 1A). The nanoparticles were spherical (e.g., DOX-AS-M-NPs, Figure 1B). The release of the DOX from the nanoparticles was biphasic; a typical burst release phase was followed by a slower release phase (Figure 1C). The cytotoxicity of the DOX-loaded nanoparticles was tested in B16-F10 mouse melanoma cells and in J774A.1 mouse macrophage cells. In B16-F10 cells, the IC_{50} values of all DOX-loaded nanoparticles were not different from one another, but they were significantly higher than that of free DOX (Figure 1D). In J774A.1 cells, except the DOX-M-NPs, the IC_{50} values of all other DOX-loaded nanoparticles were not different from that of free DOX (Figure 1D). However, after the DOX-AS-M-NPs were preincubated in a pH 6.8 buffer for 6 h to facilitate the shedding of the PEG chains before they were added into cells, their IC_{50} value in J774A.1 cells was significantly

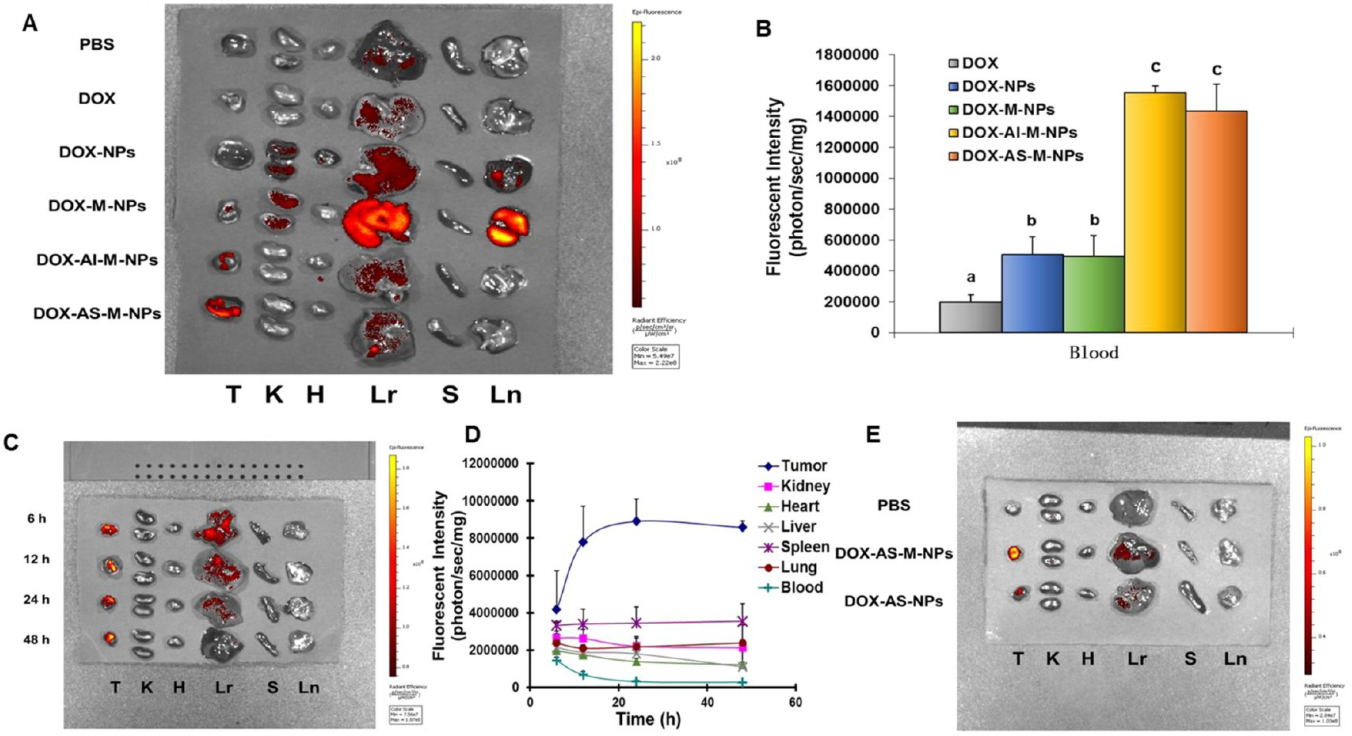

Figure 3. Biodistribution of DOX in B16-F10 tumor-bearing mice. Representative *ex vivo* fluorescence images of B16-F10 tumors and other major organs (A) and mean fluorescent intensity of DOX in mouse blood samples (B), 6 h after mice were i.v. injected with PBS, DOX, DOX-NPs, DOX-M-NPs, DOX-AI-M-NPs, or DOX-AS-M-NPs ($^{a-c}p < 0.05$). (C) Representative *ex vivo* images of B16-F10 tumors and other major organs 6, 12, 24, or 48 h after mice were i.v. injected with DOX-AS-M-NPs. (D) Mean fluorescent intensity of DOX in tumors, organs, and blood at various time points after mice were i.v. injected with DOX-AS-M-NPs. (E) Representative *ex vivo* images of B16-F10 tumors and other major organs 6 h after mice were injected with DOX-AS-M-NPs or DOX-AS-NPs. Imaging was repeated in at least 3 mice, with similar trends (T = tumor, K = kidneys, H = heart, Lr = liver, S = spleen, and Ln = lung).

decreased (by more than 50%) (Figure 1D). The cytotoxicity of DOX-AS-M-NPs after preincubation at pH 6.8 was evaluated only in J774A.1 cells because there is evidence that the murine macrophages cells express mannose receptor.[34,39]

***In Vitro* Cellular Uptake of DOX-Loaded Nanoparticles by J774A.1 Macrophages.** To verify the surface modification of DOX-nanoparticles (i.e., PEGylation and/or mannose-modification), the uptakes of various DOX-loaded nanoparticles, DOX-NPs, DOX-M-NPs, DOX-AI-M-NPs, and DOX-AS-M-NPs, by J774A.1 mouse macrophages were evaluated microscopically after the nanoparticles were preincubated in PBS (pH 6.8) for 6 h. A minimum 6 h of incubation is needed for the shedding of 50% of the PEG chains.[34] Without the 6 h preincubation at pH 6.8, only the uptake of the DOX-M-NPs was extensive (Figure 2A). However, after 6 h of preincubation, the cellular uptake of the DOX-AS-M-NPs, but not the DOX-AI-M-NPs, was significantly increased to a level similar to that of the DOX-M-NPs (Figure 2A).

The red fluorescent signals in Figure 2A were from the DOX and were an indirect indication of the uptake of the DOX-nanoparticles. A further step was taken by labeling the AS-M-NPs with fluorescein (FITC was chemically conjugated to PLGA molecules) to directly observe the cellular uptake of the nanoparticles. As shown in Figure 2B, DOX (red fluorescence signal) was observed in the cytoplasm of cells in 20 min, and within 1 h after incubation, it was in both cytoplasm and cell nuclei (i.e., overlap of red and blue signals). FITC-labeled nanoparticles (green signals) were observed in the cytoplasm in 20 min as well, and the fluorescence intensity in the cytoplasm was increased as the incubation time was increased (to 1 h) (Figure 2B). However, the green fluorescence signals remained in the cytoplasm, not detectable in the cell nuclei (Figure 2B). The DOX that accumulated in the cell nuclei may be released from the DOX-AS-M-NPs before and/or after the cellular internalization of the nanoparticles.

Biodistribution of Doxorubicin-Loaded Nanoparticles with Various Surface-Modifications in Tumor-Bearing Mice. To evaluate the extent to which the AS-M-NPs can deliver DOX into tumors, while minimizing its accumulation in MPS organs (e.g., liver and spleen), the distribution of DOX in tumors, blood, and major organs in C57BL/6 mice with pre-established subcutaneous (s.c.) B16-F10 tumors was analyzed after free DOX or DOX-nanoparticles were i.v. injected into the mice. As shown in Figure 3A (and Figure S1, Supporting Information), in mice that were injected with DOX-NPs or DOX-M-NPs, especially the DOX-M-NPs, significant DOX accumulation was observed in mouse liver, spleen, lung, and kidneys, but not in tumors, 6 h after the injection. In mice that were injected with the DOX-AI-M-NPs, DOX distribution in the liver, spleen, lung, and kidneys of the mice was reduced, but increased in tumor (Figures 3A and S1, Supporting Information). In mice that were injected with the DOX-AS-M-NPs, DOX distribution in tumor was further increased, as compared to in mice that were injected with DOX-AI-M-NPs (Figures 3A and S1, Supporting Information). Shown in Figure 3B are the fluorescence intensities of DOX in the mouse blood 6 h after mice were injected with free DOX or various DOX-nanoparticles. The fluorescence intensity was higher in mice that were injected with DOX-AI-M-NPs or DOX-AS-M-NPs

dx.doi.org/10.1021/mp500565q | *Mol. Pharmaceutics* 2014, 11, 4425−4436

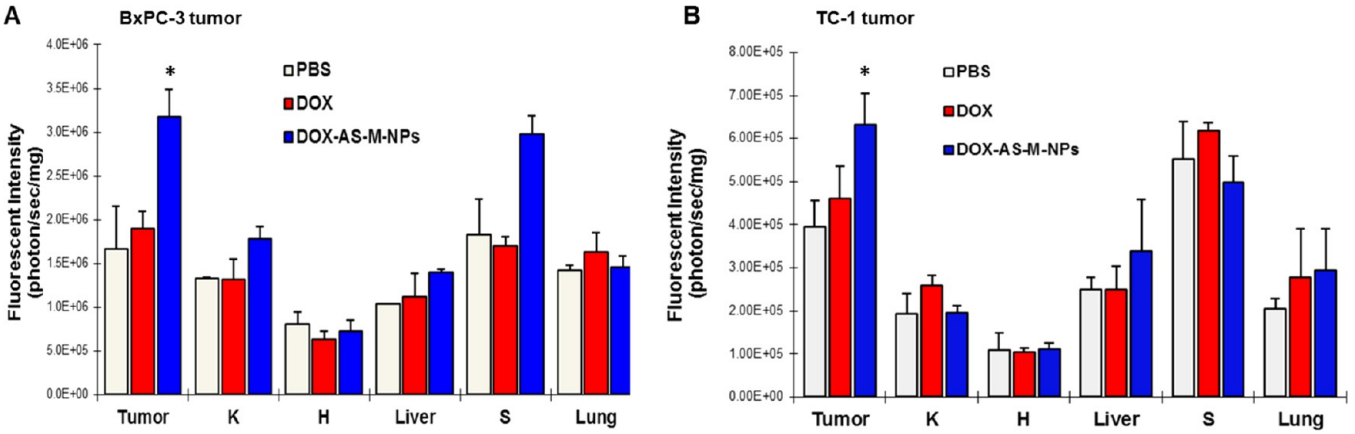

Figure 4. (A) Relative fluorescence intensities of DOX in tumors and major organs of athymic nude mice 6 h after they were i.v. injected with DOX-AS-M-NPs or free DOX. (B) Relative fluorescence intensities of DOX in tumors and major organs of C57BL/6 mice 12 h after they were i.v. injected with DOX-AS-M-NPs or free DOX. Imaging was repeated in 2−3 mice/group (K = kidneys, H = heart, and S = spleen) (*$p < 0.05$, DOX-AS-M-NPs, vs DOX or PBS in tumors).

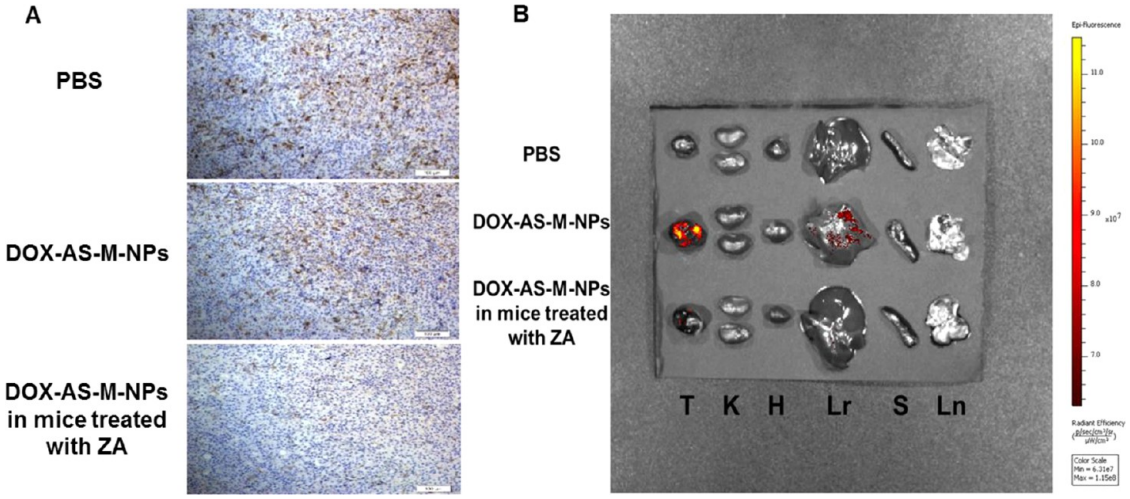

Figure 5. (A) Representative images of B16-F10 tumors stained with RM0029-11H3. Tumor-bearing mice were treated, or not, with zoledronic acid (ZA). (B) Representative *ex vivo* images of B16-F10 tumors and other major organs 6 h after mice were injected with DOX-AS-M-NPs. Prior to the injection of DOX-AS-M-NPs, one group of mice was treated with ZA (T = tumor, K = kidneys, H = heart, Lr = liver, S = spleen, and Ln = lung).

and relatively lower in mice that were injected with the DOX-NPs or DOX-M-NPs (Figure 3B). Shown in Figures 3C−D (and Figure S2, Supporting Information) are the biodistribution of the DOX-AS-M-NPs in s.c. B16-F10 tumor-bearing mice 6, 12, 24, and 48 h after i.v. injection. The fluorescence intensity of DOX-AS-M-NPs peaked in tumors about 24 h after i.v. injection, whereas the contents DOX-AS-M-NPs in blood and other organs slowly decreased as a function of time (Figures 3C,D and S2, Supporting Information).

In order to verify the function of the mannose-modification on the biodistribution of the nanoparticles, the biodistribution of the DOX-AS-M-NPs in B16-F10 tumor-bearing mice was compared with that of the DOX-AS-NPs. The accumulation of DOX in tumors in mice that were i.v. injected with the DOX-AS-NPs was significantly lower than in mice that were i.v. injected with the DOX-AS-M-NPs (Figures 3E and S3, Supporting Information).

Finally, to confirm that the DOX-AS-M-NPs are effective in delivering DOX into tumors other than the B16-F10 tumors, athymic nude mice with s.c. injected BxPC-3 human pancreatic tumor cells and C57BL/6 mice with s.c. injected TC-1 mouse lung cancer cells were used. As shown in Figure 4, DOX-AS-M-NPs significantly increased the delivery of DOX in the BxPC-3 tumors (Figure 4A) and TC-1 tumors (Figure 4B), as compared to free DOX.

Effect of the Depletion of TAMs on the Biodistribution of the DOX-AS-M-NPs in Tumor-Bearing Mice. To understand the role of TAMs in the AS-M-NPs' ability to target DOX into tumors, B16-F10 tumor-bearing mice were treated with zoledronic acid to reduce the macrophage population, including TAMs. Immunohistochemical staining confirmed the reduction of $CD206^+$ staining (an M2 macrophage marker) in tumors in mice that were treated with zoledronic acid (Figure 5A). The accumulation of DOX-AS-M-NPs in tumors in mice that were treated with zoledronic acid was significantly decreased, as compared to that in mice that were not treated with zoledronic acid (Figures 5B and S4, Supporting Information).

Uptake of DOX-AS-M-NPs by TAMs in B16-F10 Tumor-Bearing Mice. To test whether DOX-AS-M-NPs increase the uptake of DOX by TAMs, B16-F10 tumor-bearing mice were i.v. injected with free DOX or various DOX-

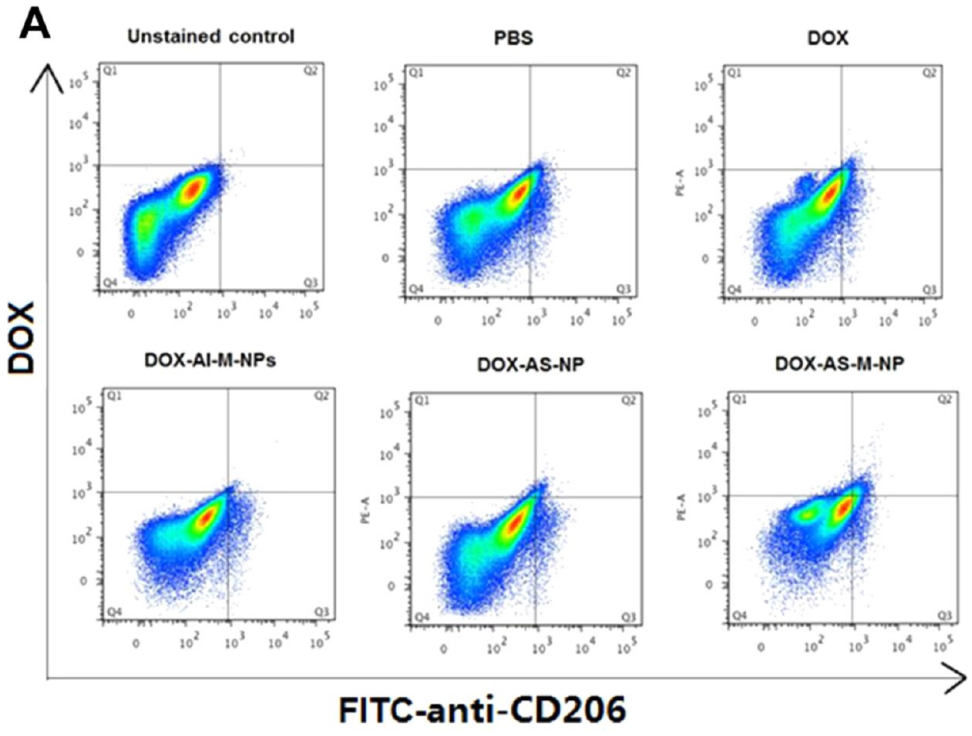

B

Group	DOX$^+$/CD206$^+$ (%)
PBS	3.98 ± 1.88 [a]
DOX	12.08 ± 3.73 [b]
AI-M-NP	12.43 ± 3.65 [b]
AS-NP	17.33 ± 4.05 [b]
AS-M-NP	34.16 ± 5.55 [c]

Figure 6. Uptake of DOX by CD206$^+$ cells in B16-F10 tumors 6 h after tumor-bearing mice were i.v. injected with free DOX or various DOX-nanoparticles. (A) Representative flow cytometric graphs of single tumor cell suspensions after stained with FITC-labeled anti-CD206. (B) The percentage of CD206$^+$ cells in B16-F10 tumors that took up DOX (i.e., DOX$^+$/CD206$^+$%). Data are mean ± SEM from at least 3 mice ($^{a-c}p < 0.05$).

nanoparticles, and the percent of CD206$^+$ cells that contained DOX (i.e., DOX$^+$/CD206$^+$%) was measured using flow cytometry 6 h after injection. As shown in Figure 6A,B, the percent of DOX$^+$/CD206$^+$ cells in tumors in mice that were i.v. injected with DOX-AS-M-NPs was significantly higher than in mice that were injected with free DOX, DOX-AI-M-NPs, or DOX-AS-NPs. In fact, it was 2−3-fold higher in tumors in mice that were injected with the DOX-AS-M-NPs than with other nanoparticles or free DOX (Figure 6B).

***In Vivo* Antitumor Activity of the DOX-AS-M-NPs.** Because the DOX-AS-M-NPs were shown to be more effective than other nanoparticles in delivering DOX into tumors, while minimizing the accumulation of DOX in MPS organs such as liver, the antitumor activity of DOX-AS-M-NPs was evaluated in B16-F10 tumor-bearing mice and compared to that of free DOX. B16-F10 tumors in mice that were i.v. injected with the DOX-AS-M-NPs grew significantly slower than in mice that were injected with free DOX at an identical DOX dose (Figure 7A). At the end of the study (i.e., 16 days after tumor cell injection), the mean weight of tumors in mice that were treated with DOX-AS-M-NPs was about 50% of that in mice that were treated with free DOX, less than 20% of that in mice left untreated (Figure 7B). Shown in Figure 7C are digital images of tumors at the end of the study, and the mean body weights of the mice during the treatment period are in Figure 7D.

Tumors in mice that were injected with sterile PBS (i.e., negative control) showed large cell nuclei and small intercellular spaces, with necrosis and hemorrhage rarely observable (H&E), while CD31$^+$ (an angiogenesis maker) and BrdU$^+$ staining (a cell proliferation marker) were extensive (Figure 7E). Tumors in mice that were treated with free DOX had some necrotic areas and small hemorrhagic regions, and CD31$^+$ and BrdU$^+$ staining remained extensive (Figure 7E). In contrast, tumors in mice that were treated with DOX-AS-M-

dx.doi.org/10.1021/mp500565q | *Mol. Pharmaceutics* 2014, 11, 4425−4436

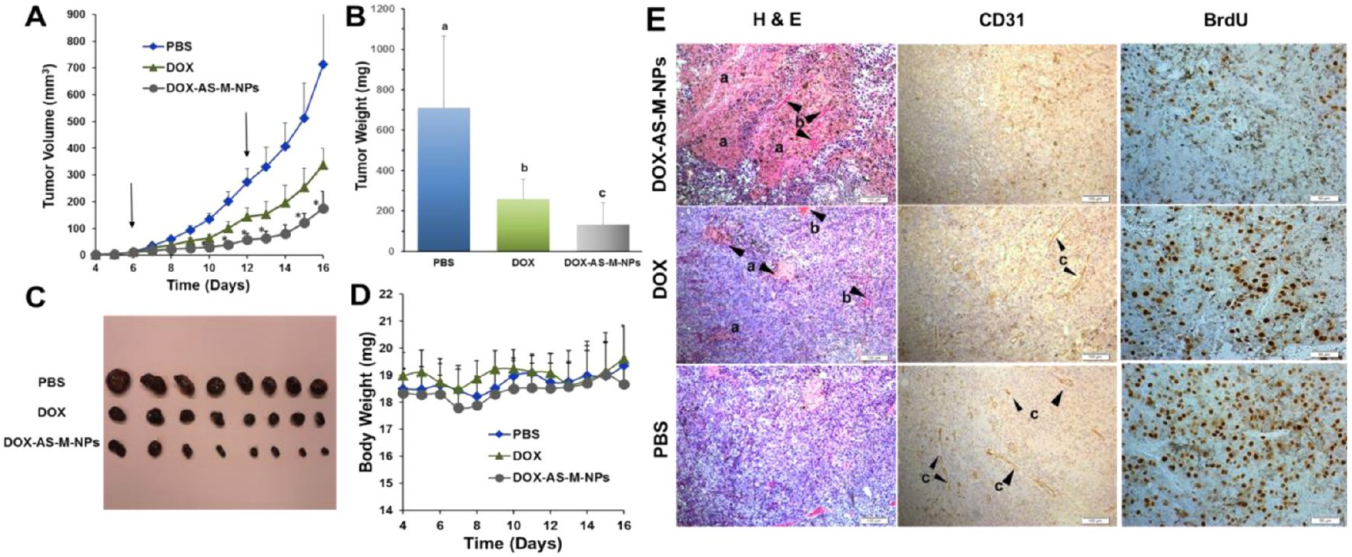

Figure 7. *in vivo* antitumor activity of DOX-AS-M-NPs. (A) Growth curves of B16-F10 tumors in C57BL/6 mice that were treated with DOX-AS-M-NPs (●) or free DOX (▲). B16-F10 tumor cells were injected in mice on day 0. Arrows indicate days on which mice were treated (*$p < 0.05$, DOX vs DOX-AS-M-NPs). Mean weight (B) and digital photographs (C) of tumors on day 16 (in panel B, [a,b]$p < 0.05$). (D) Mouse body weight. (E) Representative micrographs of tumors stained with H&E, anti-CD31 antibody, or anti-BrdU antibody ([a]necrotic areas, [b]hemorrhagic regions, and [c]blood vessels). For H&E and anti-CD31 staining, bar = 100 μm; for anti-BrdU staining, bar = 50 μm. In panels A, B, and D, data are mean ± SEM ($n = 8$).

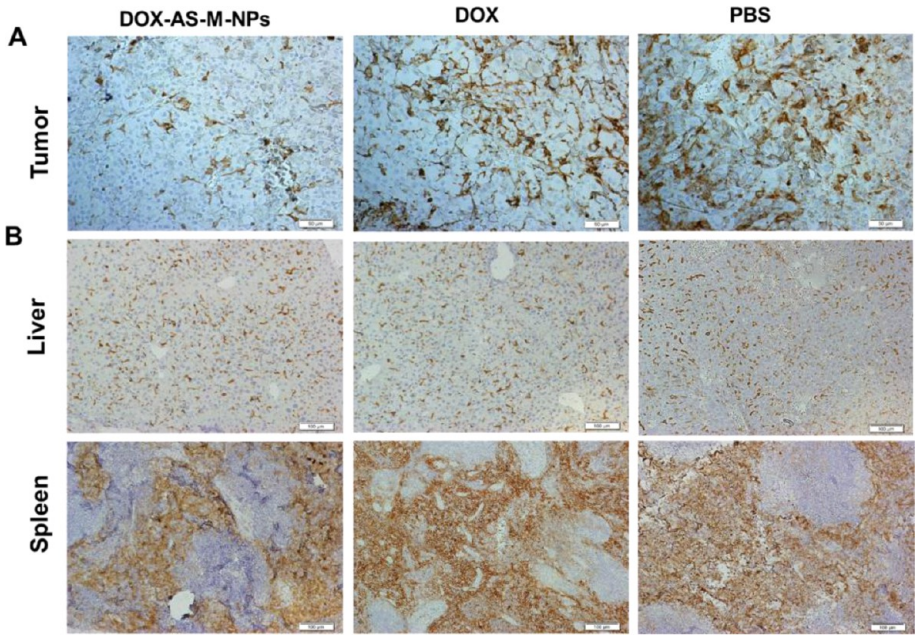

Figure 8. Representative micrographs of (A) tumor tissues stained with anti-CD206 antibody (bar = 50 μm) and (B) liver and spleen tissues stained with RM0029-11H3 (bar = 100 μm).

NPs showed numerous necrotic and hemorrhagic areas, with decreased $CD31^+$ staining and $BrdU^+$ staining (Figure 7E).

Effect of Treatment with DOX-AS-M-NPs on TAMs and on Macrophages in Liver and Spleen. To evaluate the effect of the DOX-AS-M-NPs on TAMs and macrophages in MPS, the tumor, liver, and spleen tissues from B16-F10 tumor-bearing mice that were treated with DOX-AS-M-NPs were stained with anti-CD206 (an M2 macrophage marker) or RM0029-11H3 (a pan-macrophage marker). Mice were treated with DOX-AS-M-NPs or free DOX at 6 and 12 days after tumor cell injection, and tissues were collected 4 days after the second treatment. As shown in Figure 8A, the extent of $CD206^+$ staining was significantly lower in tumors in mice that were treated with DOX-AS-M-NPs than in mice that were treated with free DOX or left untreated. However, there was no apparent difference in the extents of $RM0029\text{-}11H3^+$ staining in the liver and spleen in mice that were treated with DOX-AS-M-NPs or free DOX (Figure 8B).

■ DISCUSSION

Traditionally, active tumor-targeting is focused on exploiting receptors and proteins that are overexpressed by tumor cells or

dx.doi.org/10.1021/mp500565q | *Mol. Pharmaceutics* 2014, 11, 4425−4436

molecules that are overexpressed in tumor neovasculature.[40,41] Recently, there is increasing interest in exploring other cellular or noncellular components in tumor tissues, such as immune cells, fibroblasts, and extracellular matrix materials, for active tumor targeting.[42−44] TAMs are critical in tumors.[8] In fact, there have been some efforts in utilizing TAMs as a target for tumor imaging.[45,46] Targeting of TAMs instead of tumor cells has many advantages. Altering the tumor microenvironment that is involved in tumor angiogenesis and progression could markedly decrease metastasis, gaining better response to tumor resistance.[47,48] In addition, since TAMs exist mainly in the stroma of many tumors,[6,8] targeting of TAMs could be an effective antitumor strategy for a wide variety of tumors. Our data indicated that acid-sensitive sheddable PEGylation and mannose-modification of PLGA nanoparticles could increase the distribution of the PLGA nanoparticles in tumor tissues via interaction with TAMs while decreasing their accumulation in MPS organs such as liver.

As shown in Figure 3A, upon i.v. injection, free DOX hardly accumulated in tumors and major organs such as liver, spleen, heart, lung, and kidneys. The un-PEGylated DOX-NPs mainly accumulated in MPS organs such as liver, likely due to opsonization.[49] DOX-M-NPs were un-PEGylated, but surface-modified with mannose, and their accumulation in mouse liver, lung, and kidneys were further increased, as compared to DOX-NPs, likely because of the presence of MR-expressing macrophages in those organs as well.[50,51] Both DOX-AS-M-NPs and DOX-AI-M-NPs are PEGylated, and as expected, their distributions in major organs such as liver, lung, and kidneys were significantly decreased, but increased in tumor tissues (Figure 3A), and data in Figure 3B indicate that PEGylation increased the blood circulation time of the nanoparticles. Importantly, compared to DOX-AI-M-NPs, the distribution of DOX-AS-M-NPs in tumor was significantly higher, demonstrating the importance of acid-sensitive sheddable PEGylation in increasing the delivery of the nanoparticles into tumors. In order to understand the significance of surface-modification with mannose on the nanoparticles' ability to target tumors, the biodistribution of DOX-AS-M-NPs and DOX-AS-NPs were compared, and data in Figure 3E showed that the tumor accumulation of DOX-AS-M-NPs was significantly higher than that of DOX-AS-NPs, confirming that both acid-sensitive sheddable PEGylation and surface-modified with mannose are required for successful targeting of the DOX-NPs into tumors.

Data in Figure 4 showed that upon i.v. injection DOX-AS-M-NPs increased the delivery of DOX into s.c. BxPC-3 tumors in athymic nude mice and s.c. TC-1 tumors in C57BL/6 mice. The observed relatively higher accumulation in spleen was likely related to the relatively higher background fluorescence signal in the spleen (especially in the TC-1 tumor bearing mice (Figure 4B)), as compared to in other organs tested. A similar trend was also observed when tested in male nude mice with orthotopic Panc-1 human pancreatic tumors and in female nude mice with orthotopic MDA-MB-231 human breast tumors (data not shown). Therefore, the AS-M-NPs' ability to increase the biodistribution of molecules carried by them into tumors is not limited to the B16-F10 tumors. TAMs are critical for the AS-M-NPs to target tumors, and thus, the distribution of AS-M-NPs in different tumors will likely be affected by the population of TAMs in the tumors. B16-F10 tumors in C57BL/6 mice reportedly contain only 6−8% of TAMs.[52] Therefore, the AS-M-NPs will likely be more effective in targeting tumors that contain a higher population of TAMs.

Zoledronic acid belongs to a group of bisphosphonates, which are often used to reduce macrophage population in mouse models.[37] Data in Figure 5B showed that the distribution of DOX-AS-M-NPs in tumors in mice that were treated with zoledronic acid was significantly reduced, as compared to in similar tumor-bearing mice that were not treated with zoledronic acid, demonstrating that TAMs are required for the AS-M-NPs to successfully improve the distribution of DOX into tumors. In fact, DOX-AS-M-NPs increased the uptake of DOX by TAMs in B16-F10 tumor-bearing mice by 2−3-fold, as compared to DOX-AI-M-NPs or DOX-AS-NPs (Figure 6), further indicating that the interaction between the mannose on the surface of the DOX-AS-M-NPs and TAMs after acid-sensitive shedding of the PEG chains from the nanoparticles in tumor tissues is critical for the enhanced delivery of DOX into tumors.

Data in Figure 7 showed that DOX-AS-M-NPs are significantly more effective than free DOX in controlling tumor growth. In addition, the DOX-AS-M-NPs were also more effective than free DOX in suppressing angiogenesis ($CD31^+$ staining) and cell proliferation ($BrdU^+$ staining) in tumor tissues (Figure 7E). The stronger antitumor activity of the DOX-AS-M-NPs is likely in part due to the nanoparticle's ability to increase the delivery of DOX into tumors (Figure 3A). However, it remains unknown to what extent the stronger antitumor activity of the DOX-AS-M-NPs can be attributed to their ability to reduce the TAM population in tumors (Figure 8A). *In vitro* cytotoxicity data showed that DOX-AS-M-NPs were cytotoxic not only to B16-F10 tumor cells, but also to the J774A.1 macrophages, and shedding of the PEG chains on the DOX-AS-M-NPs significantly increased the nanoparticle's cytotoxicity to J774A.1 cells (Figure 1D). In addition, data in Figure 6 showed that, in B16-F10 tumor-bearing mice, i.v. injection of DOX-AS-M-NPs almost doubled the percentage of TAMs that took up DOX, as compared to i.v. injection of free DOX. Therefore, the strong antitumor activity of the DOX-AS-M-MPs is likely related to their ability to reduce TAM population in tumors. It is possible that B16-F10 tumors with a reduced population of TAMs are smaller than the same B16-F10 tumors with a normal population of TAMs. In addition, since TAMs promote tumor cell proliferation and induce immune suppression, a reduction of TAM population in tumors may also have contributed to the slower tumor growth in mice that were treated with DOX-AS-M-NPs. Of course, although DOX-AS-M-NPs increased the delivery of DOX into TAMs (Figure 6), it is unlikely that all the DOX-AS-M-NPs that reached the tumor were taken up by TAMs. Some DOX-AS-M-NPs that were delivered to tumor tissues were likely taken up by B16-F10 tumor cells. In addition, some DOX that was released from the DOX-AS-M-NPs, before or after the nanoparticles reached tumors, may also have been taken up by tumor cells. Therefore, the mechanism underlying the strong antitumor activity of the DOX-AS-M-NPs is expected to be multifactorial. For example, the DOX-AS-M-NPs were also more effective than DOX alone in inhibiting angiogenesis and cell proliferation in tumors (Figure 7E). It was noted that extensive necrosis was present in tumors in mice treated with DOX-AS-M-NPs (Figure 7E). Low concentrations of DOX induce necrosis, instead of apoptosis.[53] It is possible that the DOX that was slowly released from the DOX-AS-M-NPs maintained a low concentration of DOX in the tumor tissues and caused the significant necrosis.

Shown in Figure 8 are the micrographs of tumor, liver, and spleen tissues of B16-F10 tumor-bearing mice after the tissues were stained with anti-CD206 (an M2 macrophage marker) or RM0029-11H3 (a pan-macrophage marker). Compared to the tumor tissues from mice treated with free DOX or left untreated, the extent of $CD206^+$ staining was significantly decreased in tumors in mice that were treated with DOX-AS-M-NPs (Figure 8A), demonstrating DOX-AS-M-NPs' ability to reduce TAM population in tumor tissues. Importantly, the extents of RM0029-11H3-positive staining in both liver and spleen of mice that were treated with DOX-AS-M-NPs appear not different from that in mice treated with free DOX or left untreated (Figure 8B), indicating that the DOX-AS-M-NPs did not significantly affect the total macrophage population in MPS organs such as liver and spleen.

Many compounds including the bisphosphonate zoledronic acid can be used to deplete TAMs.[54] However, zoledronic acid also significantly affects macrophages that do not reside in tumors. The AS-M-NPs are advantageous because they can target tumors and TAMs but have only minimum effects on macrophages that are not tumor-associated. Of course, since macrophages are white blood cells differentiated from monocytes, arising from progenitor cells in the bone marrow,[55] there is the possibility that 4 days after the second treatment of the B16-F10 tumor-bearing mice with DOX-AS-M-NPs any major effects that the DOX-AS-M-NPs may have had on macrophages in MPS organs were restored, whereas the TAM population in tumors may take a longer time to replenish. More experiments will need to be carried out to study the effect of the DOX-AS-M-NPs on the dynamics of macrophages in tumor and nontumor tissues in the future. Nonetheless, when fully developed, the TAM-targeting nanoparticle platform can potentially be applied to deliver cytotoxic agents or macrophage-modulating agents into tumors to decouple the interaction between TAMs and tumor cells, making the tumor microenvironment less favorable for tumor growth, but more favorable for chemotherapy.

CONCLUSIONS

We demonstrated that surface-modification of PLGA nanoparticles with acid-sensitive sheddable PEG molecules and mannose as a ligand of MR, which is overexpressed on TAMs, allows the nanoparticles to effectively target DOX into tumors. The targeting is dependent on the presence of sufficient TAMs in tumors. Compared to free DOX, DOX carried by the acid-sensitive sheddable PEGylated, mannose-modified PLGA nanoparticles more effectively inhibited tumor growth, reduced TAM population in tumors, but showed no or only minimum effect on the macrophage population in MPS.

ASSOCIATED CONTENT

Supporting Information

Biodistribution study images. This material is available free of charge via the Internet at http://pubs.acs.org.

AUTHOR INFORMATION

Corresponding Author

*Address: The University of Texas at Austin, Dell Pediatric Research Institute, 1400 Barbara Jordan Boulevard, Austin, Texas 78723, United States. Tel: (512) 495-4758. Fax: (512) 471-7474. E-mail: zhengrong.cui@austin.utexas.edu.

Notes

The authors declare no competing financial interest.

ACKNOWLEDGMENTS

This work was supported in part by grants from the U.S. National Cancer Institute grant (CA135274), National Natural Science Foundation of China (81460454), and Inner Mongolia Natural Science Funds (2014ZD05) (to Z.C.). Y.W.N. was supported by a doctoral scholarship from the Egyptian Ministry of Higher Education. A.M.A. is a King Abdullah International Medical Research Center (KAIMRC) scholar and is supported by the KAIMRC scholarship program.

REFERENCES

(1) Quail, D. F.; Joyce, J. A. Microenvironmental regulation of tumor progression and metastasis. *Nat. Med.* **2013**, *19* (11), 1423−37.
(2) Lin, Y.; Wei, C.; Liu, Y.; Qiu, Y.; Liu, C.; Guo, F. Selective ablation of tumor-associated macrophages suppresses metastasis and angiogenesis. *Cancer Sci.* **2013**, *104* (9), 1217−25.
(3) Qian, B. Z.; Pollard, J. W. Macrophage diversity enhances tumor progression and metastasis. *Cell* **2010**, *141* (1), 39−51.
(4) Pollard, J. W. Tumour-educated macrophages promote tumour progression and metastasis. *Nat. Rev. Cancer* **2004**, *4* (1), 71−8.
(5) Zamarron, B. F.; Chen, W. Dual roles of immune cells and their factors in cancer development and progression. *Int. J. Biol. Sci.* **2011**, *7* (5), 651−8.
(6) Whatcott, C. J.; Posner, R. G.; Von Hoff, D. D.; Han, H. Desmoplasia and Chemoresistance in Pancreatic Cancer. In *Pancreatic Cancer and Tumor Microenvironment*; Grippo, P. J., Munshi, H. G., Eds.; Transworld Research Network.: Trivandrum, India, 2012.
(7) Negus, R. P.; Stamp, G. W.; Hadley, J.; Balkwill, F. R. Quantitative assessment of the leukocyte infiltrate in ovarian cancer and its relationship to the expression of C-C chemokines. *Am. J. Pathol.* **1997**, *150* (5), 1723−34.
(8) Solinas, G.; Germano, G.; Mantovani, A.; Allavena, P. Tumor-associated macrophages (TAM) as major players of the cancer-related inflammation. *J. Leukoc. Biol.* **2009**, *86* (5), 1065−73.
(9) Mukhtar, R. A.; Nseyo, O.; Campbell, M. J.; Esserman, L. J. Tumor-associated macrophages in breast cancer as potential biomarkers for new treatments and diagnostics. *Expert Rev. Mol. Diagn.* **2011**, *11* (1), 91−100.
(10) Weizman, N.; Krelin, Y.; Shabtay-Orbach, A.; Amit, M.; Binenbaum, Y.; Wong, R. J.; Gil, Z. Macrophages mediate gemcitabine resistance of pancreatic adenocarcinoma by upregulating cytidine deaminase. *Oncogene* **2013**, 3812−9.
(11) Ellingsen, C.; Walenta, S.; Hompland, T.; Mueller-Klieser, W.; Rofstad, E. K. The microenvironment of cervical carcinoma xenografts: Associations with lymph node metastasis and its assessment by DCE-MRI. *Transl. Oncol.* **2013**, *6* (5), 607−17.
(12) Hanada, T.; Nakagawa, M.; Emoto, A.; Nomura, T.; Nasu, N.; Nomura, Y. Prognostic value of tumor-associated macrophage count in human bladder cancer. *Int. J. Urol.* **2000**, *7* (7), 263−9.
(13) Ryder, M.; Ghossein, R. A.; Ricarte-Filho, J. C.; Knauf, J. A.; Fagin, J. A. Increased density of tumor-associated macrophages is associated with decreased survival in advanced thyroid cancer. *Endocr. Relat. Cancer* **2008**, *15* (4), 1069−74.
(14) Zhang, Q. W.; Liu, L.; Gong, C. Y.; Shi, H. S.; Zeng, Y. H.; Wang, X. Z.; Zhao, Y. W.; Wei, Y. Q. Prognostic significance of tumor-associated macrophages in solid tumor: a meta-analysis of the literature. *PLoS One* **2012**, *7* (12), e50946.
(15) Kurahara, H.; Takao, S.; Maemura, K.; Mataki, Y.; Kuwahata, T.; Maeda, K.; Sakoda, M.; Iino, S.; Ishigami, S.; Ueno, S.; Shinchi, H.; Natsugoe, S. M2-polarized tumor-associated macrophage infiltration of regional lymph nodes is associated with nodal lymphangiogenesis and occult nodal involvement in pN0 pancreatic cancer. *Pancreas* **2013**, *42* (1), 155−9.

(16) Ye, X. Z.; Xu, S. L.; Xin, Y. H.; Yu, S. C.; Ping, Y. F.; Chen, L.; Xiao, H. L.; Wang, B.; Yi, L.; Wang, Q. L.; Jiang, X. F.; Yang, L.; Zhang, P.; Qian, C.; Cui, Y. H.; Zhang, X.; Bian, X. W. Tumor-associated microglia/macrophages enhance the invasion of glioma stem-like cells via TGF-beta1 signaling pathway. *J. Immunol.* **2012**, *189* (1), 444−53.
(17) Taskinen, M.; Karjalainen-Lindsberg, M. L.; Nyman, H.; Eerola, L. M.; Leppa, S. A high tumor-associated macrophage content predicts favorable outcome in follicular lymphoma patients treated with rituximab and cyclophosphamide-doxorubicin-vincristine-prednisone. *Clin. Cancer Res.* **2007**, *13* (19), 5784−9.
(18) Movahedi, K.; Schoonooghe, S.; Laoui, D.; Houbracken, I.; Waelput, W.; Breckpot, K.; Bouwens, L.; Lahoutte, T.; De Baetselier, P.; Raes, G.; Devoogdt, N.; Van Ginderachter, J. A. Nanobody-based targeting of the macrophage mannose receptor for effective in vivo imaging of tumor-associated macrophages. *Cancer Res.* **2012**, *72* (16), 4165−77.
(19) Luo, Y.; Zhou, H.; Krueger, J.; Kaplan, C.; Lee, S. H.; Dolman, C.; Markowitz, D.; Wu, W.; Liu, C.; Reisfeld, R. A.; Xiang, R. Targeting tumor-associated macrophages as a novel strategy against breast cancer. *J. Clin. Invest.* **2006**, *116* (8), 2132−2141.
(20) Fung, S.; Stella, N. Targeting endocannabinoid signaling in tumor-associated macrophages as treatment for glioblastoma multiforme. *Wiley Interdiscip. Rev. Membr. Transp. Signaling* **2014**, *3* (2), 39−51.
(21) Hagemann, T.; Lawrence, T.; McNeish, I.; Charles, K. A.; Kulbe, H.; Thompson, R. G.; Robinson, S. C.; Balkwill, F. R. "Re-educating" tumor-associated macrophages by targeting NF-kappaB. *J. Exp. Med.* **2008**, *205* (6), 1261−8.
(22) Etzerodt, A.; Maniecki, M. B.; Graversen, J. H.; Möller, H. J.; Torchilin, V. P.; Moestrup, S. K. Efficient intracellular drug-targeting of macrophages using stealth liposomes directed to the hemoglobin scavenger receptor CD163. *J. Controlled Release* **2012**, *160* (1), 72−80.
(23) Nagai, T.; Tanaka, M.; Tsuneyoshi, Y.; Xu, B.; Michie, S. A.; Hasui, K.; Hirano, H.; Arita, K.; Matsuyama, T. Targeting tumor-associated macrophages in an experimental glioma model with a recombinant immunotoxin to folate receptor beta. *Cancer Immunol. Immunother.* **2009**, *58* (10), 1577−86.
(24) Nagayoshi, R.; Nagai, T.; Matsushita, K.; Sato, K.; Sunahara, N.; Matsuda, T.; Nakamura, T.; Komiya, S.; Onda, M.; Matsuyama, T. Effectiveness of anti-folate receptor beta antibody conjugated with truncated *Pseudomonas* exotoxin in the targeting of rheumatoid arthritis synovial macrophages. *Arthritis Rheum.* **2005**, *52* (9), 2666−75.
(25) Mantovani, A.; Sozzani, S.; Locati, M.; Allavena, P.; Sica, A. Macrophage polarization: tumor-associated macrophages as a paradigm for polarized M2 mononuclear phagocytes. *Trends Immunol.* **2002**, *23* (11), 549−555.
(26) Yu, W. Y.; Liu, C. X.; Liu, Y.; Zhang, N.; Xu, W. F. Mannan-modified solid lipid nanoparticles for targeted gene delivery to alveolar macrophages. *Pharm. Res.* **2010**, *27* (8), 1584−1596.
(27) Locke, L. W.; Mayo, M. W.; Yoo, A. D.; Williams, M. B.; Berr, S. S. PET imaging of tumor associated macrophages using mannose coated Cu-64 liposomes. *Biomaterials* **2012**, *33* (31), 7785−7793.
(28) Movahedi, K.; Schoonooghe, S.; Laoui, D.; Houbracken, I.; Waelput, W.; Breckpot, K.; Bouwens, L.; Lahoutte, T.; De Baetselier, P.; Raes, G.; Devoogdt, N.; Van Ginderachter, J. A. Nanobody-based targeting of the macrophage mannose receptor for effective in vivo imaging of tumor-associated macrophages. *Cancer Res.* **2012**, *72* (16), 4165−4177.
(29) Huang, Z.; Zhang, Z. P.; Jiang, Y. C.; Zhang, D. C.; Chen, J. N.; Dong, L.; Zhang, J. F. Targeted delivery of oligonucleotides into tumor-associated macrophages for cancer immunotherapy. *J. Controlled Release* **2012**, *158* (2), 286−292.
(30) Cook, J.; Hagemann, T. Tumour-associated macrophages and cancer. *Curr. Opin. Pharmacol.* **2013**, *13* (4), 595−601.
(31) Zhu, S.; Wonganan, P.; Lansakara, P. D.; O'Mary, H. L.; Li, Y.; Cui, Z. The effect of the acid-sensitivity of 4-(*N*)-stearoyl gemcitabine-loaded micelles on drug resistance caused by RRM1 overexpression. *Biomaterials* **2013**, *34* (9), 2327−39.
(32) Matsumura, Y.; Maeda, H. A new concept for macromolecular therapeutics in cancer chemotherapy: mechanism of tumoritropic accumulation of proteins and the antitumor agent smancs. *Cancer Res.* **1986**, *46* (12 Pt 1), 6387−92.
(33) Tian, L.; Bae, Y. H. Cancer nanomedicines targeting tumor extracellular pH. *Colloids Surf., B* **2012**, *99*, 116−26.
(34) Zhu, S.; Niu, M.; O'Mary, H.; Cui, Z. Targeting of tumor-associated macrophages made possible by PEG-sheddable, mannose-modified nanoparticles. *Mol. Pharmaceutics* **2013**, *10* (9), 3525−3530.
(35) Tang, K. S.; Hashmi, S. M.; Shapiro, E. M. The effect of cryoprotection on the use of PLGA encapsulated iron oxide nanoparticles for magnetic cell labeling. *Nanotechnology* **2013**, *24* (12), 125101.
(36) Saragusti, A. C.; Bustos, P. S.; Pierosan, L.; Cabrera, J. L.; Chiabrando, G. A.; Santos, A. R.; Ortega, M. G. Involvement of the L-arginine-nitric oxide pathway in the antinociception caused by fruits of *Prosopis strombulifera* (Lam.) Benth. *J. Ethnopharmacol.* **2012**, *140* (1), 117−22.
(37) Zhang, W.; Zhu, X. D.; Sun, H. C.; Xiong, Y. Q.; Zhuang, P. Y.; Xu, H. X.; Kong, L. Q.; Wang, L.; Wu, W. Z.; Tang, Z. Y. Depletion of tumor-associated macrophages enhances the effect of sorafenib in metastatic liver cancer models by antimetastatic and antiangiogenic effects. *Clin. Cancer Res.* **2010**, *16* (13), 3420−30.
(38) Rodriguez, B. L.; Blando, J. M.; Lansakara, P. D.; Kiguchi, Y.; DiGiovanni, J.; Cui, Z. Antitumor activity of tumor-targeted RNA replicase-based plasmid that expresses interleukin-2 in a murine melanoma model. *Mol. Pharmaceutics* **2013**, *10* (6), 2404−15.
(39) Harris, N.; Super, M.; Rits, M.; Chang, G.; Ezekowitz, R. A. Characterization of the murine macrophage mannose receptor: demonstration that the downregulation of receptor expression mediated by interferon-gamma occurs at the level of transcription. *Blood* **1992**, *80* (9), 2363−73.
(40) Dai, W.; Yang, T.; Wang, X.; Wang, J.; Zhang, X.; Zhang, Q. PHSCNK-Modified and doxorubicin-loaded liposomes as a dual targeting system to integrin-overexpressing tumor neovasculature and tumor cells. *J. Drug Targeting* **2010**, *18* (4), 254−63.
(41) Sanchez, C.; El Hajj Diab, D.; Connord, V.; Clerc, P.; Meunier, E.; Pipy, B.; Payre, B.; Tan, R. P.; Gougeon, M.; Carrey, J.; Gigoux, V.; Fourmy, D. Targeting a G-protein-coupled receptor overexpressed in endocrine tumors by magnetic nanoparticles to induce cell death. *ACS Nano* **2014**, *8* (2), 1350−63.
(42) Liyanage, U. K.; Moore, T. T.; Joo, H. G.; Tanaka, Y.; Herrmann, V.; Doherty, G.; Drebin, J. A.; Strasberg, S. M.; Eberlein, T. J.; Goedegebuure, P. S.; Linehan, D. C. Prevalence of regulatory T cells is increased in peripheral blood and tumor microenvironment of patients with pancreas or breast adenocarcinoma. *J. Immunol.* **2002**, *169* (5), 2756−61.
(43) Mitchem, J. B.; Brennan, D. J.; Knolhoff, B. L.; Belt, B. A.; Zhu, Y.; Sanford, D. E.; Belaygorod, L.; Carpenter, D.; Collins, L.; Piwnica-Worms, D.; Hewitt, S.; Udupi, G. M.; Gallagher, W. M.; Wegner, C.; West, B. L.; Wang-Gillam, A.; Goedegebuure, P.; Linehan, D. C.; DeNardo, D. G. Targeting tumor-infiltrating macrophages decreases tumor-initiating cells, relieves immunosuppression, and improves chemotherapeutic responses. *Cancer Res.* **2013**, *73* (3), 1128−41.
(44) Loeffler, M.; Kruger, J. A.; Niethammer, A. G.; Reisfeld, R. A. Targeting tumor-associated fibroblasts improves cancer chemotherapy by increasing intratumoral drug uptake. *J. Clin. Invest.* **2006**, *116* (7), 1955−62.
(45) Locke, L. W.; Mayo, M. W.; Yoo, A. D.; Williams, M. B.; Berr, S. S. PET imaging of tumor associated macrophages using mannose coated 64Cu liposomes. *Biomaterials* **2012**, *33* (31), 7785−93.
(46) Daldrup-Link, H. E.; Golovko, D.; Ruffell, B.; Denardo, D. G.; Castaneda, R.; Ansari, C.; Rao, J.; Tikhomirov, G. A.; Wendland, M. F.; Corot, C.; Coussens, L. M. MRI of tumor-associated macrophages with clinically applicable iron oxide nanoparticles. *Clin. Cancer Res.* **2011**, *17* (17), 5695−704.

(47) Sounni, N. E.; Noel, A. Targeting the tumor microenvironment for cancer therapy. *Clin. Chem.* **2013**, *59* (1), 85−93.
(48) Melissa, R. J.; Frederic, J. d. S. Influence of tumour microenvironment heterogeneity on therapeutic response. *Nature* **2013**, *501* (7467), 346−354.
(49) Illum, S. L.; Davis, S. S. Effect of the nonionic surfactant poloxamer 338 on the fate and deposition of polystyrene microspheres following intravenous administration. *J. Pharm. Sci.* **1983**, *72* (9), 1086−9.
(50) Jones, C. V.; Williams, T. M.; Walker, K. A.; Dickinson, H.; Sakkal, S.; Rumballe, B. A.; Little, M. H.; Jenkin, G.; Ricardo, S. D. M2 macrophage polarisation is associated with alveolar formation during postnatal lung development. *Respir. Res.* **2013**, *14*, 41.
(51) Mandal, P.; Pratt, B. T.; Barnes, M.; McMullen, M. R.; Nagy, L. E. Molecular mechanism for adiponectin-dependent M2 macrophage polarization: link between the metabolic and innate immune activity of full-length adiponectin. *J. Biol. Chem.* **2011**, *286* (15), 13460−9.
(52) Kluza, E.; Yeo, S. Y.; Schmid, S.; van der Schaft, D. W.; Boekhoven, R. W.; Schiffelers, R. M.; Storm, G.; Strijkers, G. J.; Nicolay, K. Anti-tumor activity of liposomal glucocorticoids: The relevance of liposome-mediated drug delivery, intratumoral localization and systemic activity. *J. Controlled Release* **2011**, *151* (1), 10−7.
(53) Sugimoto, K.; Tamayose, K.; Sasaki, M.; Hayashi, K.; Oshimi, K. Low-dose doxorubicin-induced necrosis in Jurkat cells and its acceleration and conversion to apoptosis by antioxidants. *Br. J. Hamaetol.* **2002**, *118* (1), 229−38.
(54) Rogers, T. L.; Holen, I. Tumour macrophages as potential targets of bisphosphonates. *J. Transl. Med.* **2011**, *9*, 177.
(55) Gordon, S. Alternative activation of macrophages. *Nat. Rev. Immunol.* **2003**, *3* (1), 23−35.